

High-resolution digital resampling using vector rational filters

Lazhar Khriji
Faouzi Alaya Cheikh
Moncef Gabbouj
Tampere University of Technology
Signal Processing Laboratory
P.O. Box 553
FIN-33101 Tampere
Finland
E-mail: moncef@cs.tut.fi

Abstract. Rational filters are extended to multichannel signal processing and applied to image interpolation. Two commonly used decimation schemes are considered: a rectangular grid and a quincunx grid. For each decimation lattice, we propose a number of adaptive resampling algorithms based on the vector rational filter (VRF). These algorithms exhibit desirable properties such as edge and detail preservation and accurate chromaticity estimation. In these approaches, color image pixels are considered as three-component vectors in the color space. Therefore, the inherent correlation that exists between the different color components is not ignored. This leads to better image quality compared to that obtained by componentwise or marginal processing. Extensive simulations show that multichannel image processing with the proposed algorithms (VRF_L) and (VRF_d) based on l_p -norm and directional processing, respectively; significantly outperform linear and some nonlinear techniques, e.g., vector FIR median hybrid filters (VFMH). Some images interpolated using VRF_L and VRF_d are presented for qualitative comparison. These images are free from blockiness and jaggedness, confirming the quantitative results. © 1999 Society of Photo-Optical Instrumentation Engineers. [S0091-3286(99)00105-1]

Subject terms: rational filters; nonlinear interpolation; vector rational filters; adaptive processing; directional processing.

Paper SIS-02 received July 14, 1998; revised manuscript received Oct. 5, 1998; accepted for publication Oct. 5, 1998.

1 Introduction

The process of decimation or down-sampling is equivalent to intelligently discarding data. This can be informally defined as the process of representing an input image on a new sampling grid, with a lower sampling density than the original grid.¹ The goal is to reduce the amount of information transmitted through the communication channels and the local storage requirements, while preserving the image quality as much as possible. Down-sampling belongs to the class of geometric scaling procedures that also includes the reverse operation, i.e., up-sampling or up-scaling, achieved either by pixel replication or by interpolation to restore the original high-resolution image from its decimated version or for resizing or zooming a digital image. Decimation followed later by interpolation (Fig. 1) is used in many practical applications, such as progressive image transmission systems, image/video zooming, photographic enlarging, image reconstruction, optical scanners, and high-resolution printers, and in multimedia applications that require browsing or retrieval of images from the Internet or image and video databases. These tasks become more complex in the case of color images, which usually require larger storage capacity and processing time. Moreover, restoring the original colors accurately increases the computational complexity. The design of robust and good interpolators is crucial to achieving a reconstructed image with high quality.

A number of conventional interpolation techniques were proposed to increase the spatial resolution of an image (see, for instance, Refs. 2 and 3). These techniques degrade the

quality of the magnified image due to various artifacts (to which the human eye is quite sensitive), such as, blocking artifact and excessive smoothing. Such degradations worsen as the magnification ratio increases. Therefore, a tradeoff between reducing blocking artifacts and excessive smoothing should be found.⁴ Although conventional techniques are well established for univariate 2-D signals, such as gray level images, an extension of these techniques to multivariate data, such as color images, is not straightforward. Processing each color component separately fails to take into account the inherent correlation that exists between the different channels. Adaptive methods aim to avoid these problems by analyzing the local structure of the source (or original) image and using different interpolation functions with different areas of support.

In the following, we present an adaptive algorithm for color image interpolation using a new class of vector rational filters recently proposed in Refs. 5 and 6. These are applied to two different resampling, i.e., down-sampling and up-sampling, the rectangular and quincunx lattices (see Fig. 2). This new algorithm yields better interpolated images than those obtained with a number of linear and other nonlinear techniques. Among the nonlinear methods are the vector median filter⁷ and the vector directional filter.⁸ Another class of nonlinear filters that has been widely studied for signal and image processing is that of Volterra systems (see for instance Ref. 9) and particularly its subclass, polynomial filters¹⁰ and in turn its subclass quadratic filters.¹¹ Rational filters, as the name indicates, consist of the ratio of

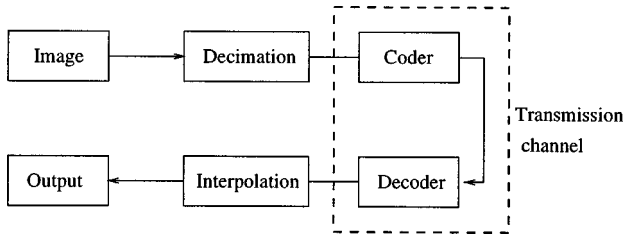


Fig. 1 Decimation/interpolation based compression system.

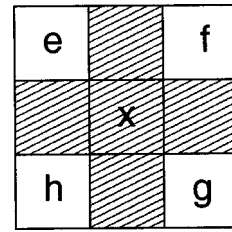


Fig. 3 A 3 × 3 mask to interpolate the sample *x* using the known data *e*, *f*, *g* and *h*.

two polynomials and were introduced by Leung and Haykin¹² based on the work of Walsh¹³ for signal detection and estimation and were later applied by Ramponi¹⁴ for image filtering and enhancement.

The paper is organized as follows. Section 2 briefly reviews rational functions. In Section 3, the definition of the vector rational filters⁵ is presented and two new interpolation schemes are discussed: the border preserving interpolator and the separable row-column interpolator. Section 4 describes an extension of the vector rational function (VRF) to directional processing. Section 5 presents extensive simulation results and a discussion on the improvement achieved by the proposed vector rational approaches. To incorporate perceptual criteria in the comparisons, the errors are measured in the uniform $L^*a^*b^*$ color space.¹⁵ Section 6 concludes the paper.

2 Rational Functions

Nonlinear approximation techniques are now commonly used due to their ability to capture complex and salient features in the processed signals. Practical approximators are simple functions (i.e., low computational complexity) that are able to represent a given signal with the required accuracy. Rational functions belong to this category. For

example, trigonometric functions are computed using rational approximating functions on a computer. More generally, a number of engineering problems such as optical transformation, interpolation of TV image sequence, input resistance of cascaded resistance networks and image propagation for two inward-facing parabolic mirrors have been found to be well represented by rational functions. These applications confirm the significance of rational functions, and hence their suitability for incorporation in the design of nonlinear filters.

Recently, rational functions were proposed as a new class of nonlinear signal processing techniques.^{12,14} The input/output relation for a rational function is given by¹⁶

$$y = \frac{a_0 + \sum_{i=1}^m a_{1i}x_i + \sum_{i=1}^m \sum_{j=1}^m a_{2ij}x_i x_j + \dots}{b_0 + \sum_{i=1}^m b_{1i}x_i + \sum_{i=1}^m \sum_{j=1}^m b_{2ij}x_i x_j + \dots}, \quad (1)$$

where x_1, x_2, \dots, x_m are the scalar inputs to the filter; y is the filter output; and a_0, b_0, a_{ij} and b_{ij} are filter parameters.

The representation described in Eq. (1) is unique up to the constant factors in the numerator and denominator polynomials. The rational function (RF) must clearly have a finite order to be useful in solving practical problems. Like polynomial functions, an RF is a universal approximator.¹² Moreover, it is able to achieve substantially higher accuracy with lower complexity and possesses better extrapolation capabilities than polynomial functions.

Ramponi proposed the rational filter and used it in different image processing tasks, such as, enhancement and filtering.¹⁴ Later, he proposed a rational filter for image interpolation¹⁷ that is able to reconstruct sharp edges accurately without ringing effects. The value of the pixel x to be interpolated according to Fig. 3 is computed as

$$x = \frac{w_{ef}(e+f) + w_{fg}(f+g) + w_{gh}(g+h) + w_{he}(h+e)}{2(w_{ef} + w_{fg} + w_{gh} + w_{he})}$$

$$= \frac{1}{W} \left(w_{ef} \frac{e+f}{2} + w_{fg} \frac{f+g}{2} + w_{gh} \frac{g+h}{2} + w_{he} \frac{h+e}{2} \right), \quad (2)$$

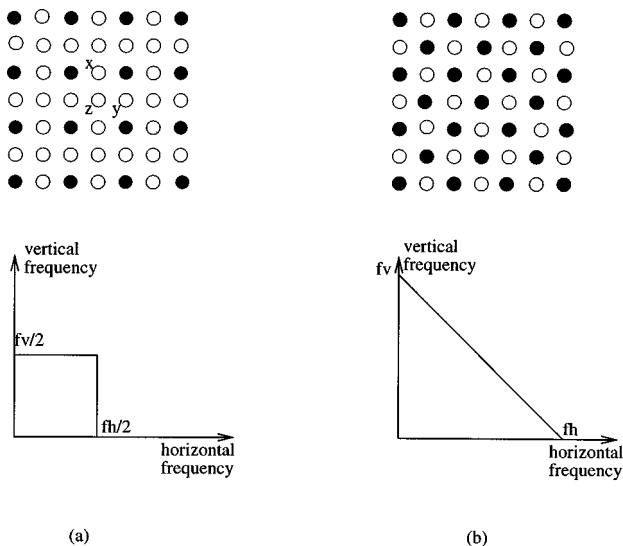


Fig. 2 (a) Rectangular decimation (factor 1/4) and its primitive bandwidth and (b) quincunx decimation (factor 1/2) and its bandwidth.

where $W = w_{ef} + w_{fg} + w_{gh} + w_{he}$. The filter coefficients are given by $w_{\alpha\beta} = 1/[8 + k(\beta - \alpha)^2]$, $\alpha, \beta \in \{e, f, g, h\}$, and k is a fixed positive constant. The parameter k controls the nonlinearity of the weights distribution.

3 VRF Based Interpolators

Straight forward application of the RFs to multichannel image processing would be based on processing the image components separately, i.e., componentwise or marginal processing. This, however, fails to exploit the inherent correlation that is usually present in multichannel images. Consequently, vector processing of multichannel images is desirable.¹⁸

By examining the expression of the 2-D scalar interpolator [Eq. (2)], one can see that the denominator is a normalizing factor when the filter window is located in a flat area [i.e., the sum of the weights w_{ef} , w_{fg} , w_{gh} and w_{he} in Eq. (2) is equal to 1] so that the filter will correspond to the identity operator in such a region. Furthermore, the numerator is a weighted sum of the horizontal and vertical neighboring input pixel pairs. The weights are nonlinear functions of the input pixel values, and they are edge sensitive since they are computed based on a gradient like operation.

The pixel differences $\beta - \alpha$, $\alpha, \beta \in \{e, f, g, h\}$, in the weights give an indication of the presence of edges in the corresponding direction *edge sensing factor*. The contribution of the average of a pixel pair having a large gray scale difference is reduced at the output to prevent edge blurring.

On one hand, pixels with similar magnitudes will have large weights and therefore the contribution of their average is enforced. Near a sharp transition, only one pair of pixels (those that are on the higher side of the edge) will have a large weight and therefore its contribution to the output will be very important. Smoothing of the transition is thus not allowed. On the other hand, in flat areas, all the surrounding pixels contribute to the output equally. In this way, sharp edges are retained and smooth flat regions are not altered.

Detecting the presence of transitions in a signal can be obtained by segmenting the pixels inside the processing window into different regions using a similarity measure. For the case of scalar signals, the difference between the pixel values is a good measure of similarity. For multichannel signals the problem of detecting transitions in the signal is a more complex one. However, some measures can be used, such as the Euclidean distance and the angles between the vectors as in vector directional filtering in Ref. 8.

Let us next define the proposed structure of the VRF.

Definition 3.1. Let $\mathbf{x}_1, \mathbf{x}_2, \dots, \mathbf{x}_m$ be the m input vectors to the filter, where $\mathbf{x}_i = [x_i^1, x_i^2, \dots, x_i^l]^T$ and $x_i^k \in \{0, 1, \dots, M\}$, M is an integer. The VRF output is given by

$$\begin{aligned} \text{VRF} = \text{RF}[\mathbf{x}_1, \mathbf{x}_2, \dots, \mathbf{x}_m] &= \frac{P(\mathbf{x}_1, \mathbf{x}_2, \dots, \mathbf{x}_m)}{Q(\mathbf{x}_1, \mathbf{x}_2, \dots, \mathbf{x}_m)} \\ &= [rf_1, rf_2, \dots, rf_l]^T, \end{aligned} \quad (3)$$

where P is a vector-valued polynomial, and Q is a scalar

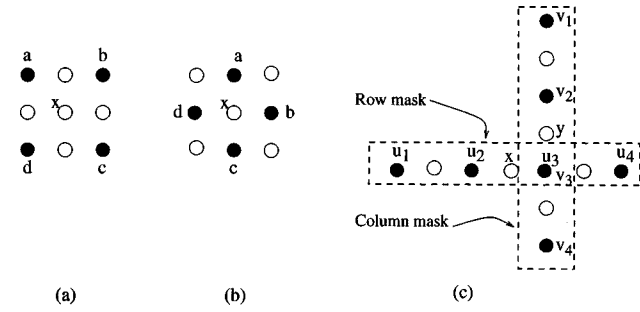


Fig. 4 (a) and (b) Border-preserving interpolator and (c) separable row-column interpolator.

polynomial. Both are functions of the input vectors. The i 'th component of the VRF output is written as

$$rf_i = \left[\frac{P_i(\mathbf{x}_1, \mathbf{x}_2, \dots, \mathbf{x}_m)}{Q(\mathbf{x}_1, \mathbf{x}_2, \dots, \mathbf{x}_m)} \right] \in \{0, 1, \dots, M\}, \quad (4)$$

where

$$\begin{aligned} P_i(\mathbf{x}_1, \mathbf{x}_2, \dots, \mathbf{x}_m) &= a_0 + \sum_{k=1}^m a_k x_k^i + \sum_{k_1=1}^m \sum_{k_2=1}^m a_{k_1 k_2} x_{k_1}^i x_{k_2}^i \\ &+ \dots, \end{aligned} \quad (5)$$

and

$$Q(\mathbf{x}_1, \mathbf{x}_2, \dots, \mathbf{x}_m) = b_0 + \sum_{j=1}^m \sum_{k=1}^m b_{jk} \|\mathbf{x}_j - \mathbf{x}_k\|_p. \quad (6)$$

Here $\|\cdot\|_p$ is the l_p -norm, and $[\alpha]$ is the integer part of α , $\alpha \in \mathcal{R}_+$; $b_0 > 0$, b_{ij} are constant, and a_{i_1, i_2, \dots, i_n} is a function of the input vectors:

$$a_{i_1, i_2, \dots, i_n} = f(\mathbf{x}_1, \mathbf{x}_2, \dots, \mathbf{x}_m). \quad (7)$$

When the vector dimension is 1, the VRF reduces to a special case of the scalar RF.

In the following, we describe two types of interpolation using VRFs: (1) a border-preserving interpolator (bidirectional interpolator) and (2) a separable row-column interpolator (unidirectional interpolator).

3.1 Border-Preserving Interpolator

With reference to Fig. 4(a), our nonlinear interpolator operates on four samples of decimated multivariate data, \mathbf{a} , \mathbf{b} , \mathbf{c} and \mathbf{d} (mask, 3×3) to reconstruct the missing sample \mathbf{x} in the central position. To weight the contributions to \mathbf{x} of its four neighboring samples, a VRF is used. The normalized weights verify two conditions. First, each weight is a positive number. Second, in a flat area (where we assume that the four neighbors of the pixel under consideration

have the same value), the sum of the weights is equal to 1, which ensures that the output is unbiased. The interpolator output is as follows:

$$\begin{aligned} \mathbf{x} &= \frac{\sum_{\{u \neq v; u, v \in (a, b, c, d)\}} w_{uv} \cdot (\mathbf{u} + \mathbf{v})}{2 \sum_{\{u \neq v; u, v \in (a, b, c, d)\}} w_{uv}} \\ &= \frac{1}{W} \left(\frac{w_{ab} + w_{ac} + w_{da}}{2} \mathbf{a} + \frac{w_{ab} + w_{bc} + w_{bd}}{2} \mathbf{b} \right. \\ &\quad \left. + \frac{w_{ac} + w_{bc} + w_{cd}}{2} \mathbf{c} + \frac{w_{bd} + w_{cd} + w_{da}}{2} \mathbf{d} \right), \end{aligned} \quad (8)$$

where $W = w_{ab} + w_{bc} + w_{cd} + w_{da} + w_{ac} + w_{bd}$. The weights are computed as follows:

$$w_{uv} = \frac{1}{12 + k \|\mathbf{v} - \mathbf{u}\|_p}, \quad (9)$$

where $\mathbf{u}, \mathbf{v} \in \{\mathbf{a}, \mathbf{b}, \mathbf{c}, \mathbf{d}\}$, and $\|\cdot\|_p$ denotes l_1 - or l_2 -norm.

3.2 Separable Row-Column Interpolator

This operator can be applied separately by row (row mask) and by column (column mask) according to Fig. 4(c). The interpolated vector \mathbf{x} is computed as follows:

$$\mathbf{x} = \alpha \mathbf{u}_2 + (1 - \alpha) \mathbf{u}_3, \quad (10)$$

where the parameter in Eq. (10) is a scalar RF of the input vectors and computed as:

$$\alpha = \frac{1 + k \|\mathbf{u}_2 - \mathbf{u}_4\|_p}{2 + k (\|\mathbf{u}_1 - \mathbf{u}_3\|_p + \|\mathbf{u}_2 - \mathbf{u}_4\|_p)}. \quad (11)$$

Thus Eq. (10) becomes:

$$\mathbf{x} = \frac{(1 + k \|\mathbf{u}_2 - \mathbf{u}_4\|_p) \mathbf{u}_2 + [1 + k (\|\mathbf{u}_1 - \mathbf{u}_3\|_p + (k - 1) \|\mathbf{u}_2 - \mathbf{u}_4\|_p)] \mathbf{u}_3}{2 + k (\|\mathbf{u}_1 - \mathbf{u}_3\|_p + \|\mathbf{u}_2 - \mathbf{u}_4\|_p)}. \quad (12)$$

Vector \mathbf{y} is computed using a similar mask but columnwise (using the \mathbf{v}_i vectors).

4 Directional Processing

The previous interpolators use the difference of the vector magnitudes as edge sensors. In the color space, transitions are also represented by angles between the color vectors. At a fixed luminance, small angles between color vectors denote ‘‘color’’ homogeneous regions; whereas, large angles indicate edges. In the following, a modified VRF is proposed in which the edge sensors rely on the angles between the color vectors instead of the difference of their magnitudes.

Color images are 2-D three-channel signals where each pixel can be represented as a vector in the 3-D color space. Color image pixels are thus regarded as vectors in the color cube, as shown in Fig. 5. The points marked with a cross \times

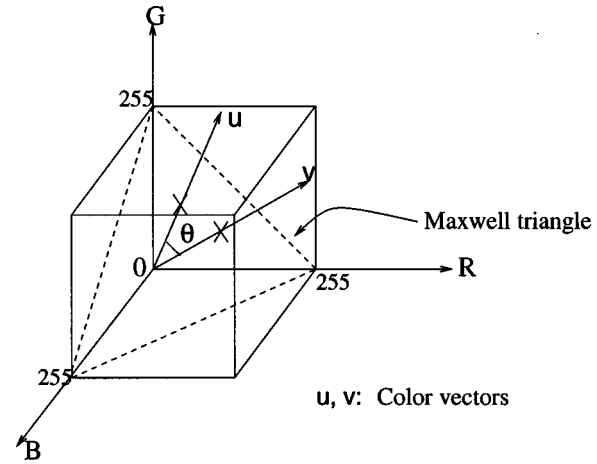


Fig. 5 Vectorial representation of the color image pixels in the RGB color space.

denote the intersection points of the color vectors with the *Maxwell triangle* (the triangle drawn between the three primaries, R, G, B), and θ represents the angle between two vectors \mathbf{u} and \mathbf{v} .

The angle between the directions of the color vectors is now used as the edge sensitivity measure. The goal is to sustain the sharpness of the interpolated image by preserving the transitions detected in the color space. The weights of the modified VRF are computed as follows.

4.1 Border-Preserving Angle-Based Interpolator

The border-preserving interpolator has the same expression as in Eq. (8) in the previous section, except that the weights in Eq. (9) are computed as follows:

$$w_{uv} = \frac{1}{12 + k \theta^2(\mathbf{u}, \mathbf{v})}, \quad (13)$$

where $\mathbf{u}, \mathbf{v} \in \{\mathbf{a}, \mathbf{b}, \mathbf{c}, \mathbf{d}\}$, and $\theta(\mathbf{u}, \mathbf{v})$ denotes the angle between the two vectors \mathbf{u} and \mathbf{v} (expressed in radians) and measured on the plane defined by the *Maxwell triangle* (see Fig. 5) and bounded by:

$$0 \leq \theta(\mathbf{u}, \mathbf{v}) \leq \frac{\pi}{2}. \quad (14)$$

4.2 Separable Row-Column Angle-Based Interpolator

The interpolated vector \mathbf{x} is computed as in Eq. (10) but using the following expression for parameter α :

$$\alpha = \frac{1 + k \theta^2(\mathbf{u}_2, \mathbf{u}_4)}{2 + k [\theta^2(\mathbf{u}_1, \mathbf{u}_3) + \theta^2(\mathbf{u}_2, \mathbf{u}_4)]}. \quad (15)$$

5 Experimental Results

To assess the performance of the proposed interpolators, two color images (‘‘Lena’’ image of size 480×512 and a

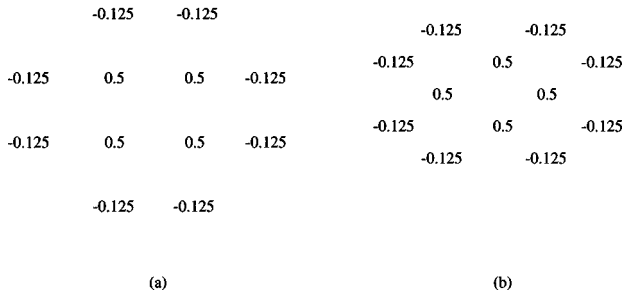


Fig. 6 FIR filter coefficients used in VFMH filter: (a) FIR1 and (b) FIR2.

“Peppers” image of size 512×512) are decimated in two different ways: (1) a rectangular decimation with a factor of $1/16$ [see Fig. 2(a)] (factor $1/4$ is used here for illustration), and (2) quincunx decimation with a factor $1/2$ [see Fig. 2(b)]. Only the points indicated in black in Fig. 2 are retained from the decimation process in each of the two decimation schemes.

The full size images are then reconstructed using the following filters: a cubic convolution (CC) interpolator; a bilinear interpolator (BL); a vector finite impulse response (FIR) median hybrid (VFMH) filter, as proposed in Ref. 19 where an FIR filter with 12 coefficients was used; and the proposed VRFs. The missing \mathbf{x} -vectors (see Fig. 4) were computed by a two-step interpolation scheme:

1. For Fig. 4(a),

$$X = VM\{\mathbf{a}, \mathbf{b}, \mathbf{c}, \mathbf{d}, \mathbf{V}_{D1}, \mathbf{V}_{D2}, \mathbf{V}_{FIR1}\}, \quad (16)$$

where $\mathbf{V}_{D1} = (\mathbf{a} + \mathbf{c})/2$, $\mathbf{V}_{D2} = (\mathbf{b} + \mathbf{d})/2$ and the coefficients of \mathbf{V}_{FIR1} are given in Fig. 6(a).

2. For Fig. 4(b),

$$X = VM\{\mathbf{a}, \mathbf{b}, \mathbf{c}, \mathbf{d}, \mathbf{V}_V, \mathbf{V}_H, \mathbf{V}_{FIR2}\} \quad (17)$$

where $\mathbf{V}_V = (\mathbf{a} + \mathbf{c})/2$, $\mathbf{V}_H = (\mathbf{b} + \mathbf{d})/2$, and the coefficients of \mathbf{V}_{FIR2} are given by Fig. 6(b).

For marginal rational interpolator (Marginal RF), the border-preserving interpolator is used and applied componentwise.

For VRFs using the l_2 -norm (VRF_L), the related adaptive algorithms are as follows.

- **VRF1_L** (*Border-preserving interpolation*): The algorithm has two steps:

Step 1. According to Fig. 2(a), compute the unknown vectors \mathbf{z} by applying Eq. (8) with the cross-shaped mask shown in Fig. 4(a).

Step 2. Compute the missing vectors \mathbf{x} and \mathbf{y} using the original vectors and the \mathbf{z} vectors computed in step 1, by applying Eq. (8) with the plus-shaped mask presented in Fig. 4(b).

- **VRF2_L** (*Separable row-column interpolation*): With reference to Fig. 2(a) and Fig. 4(c):

Step 1. Apply Eq. (10) to the row mask to interpolate the \mathbf{x} vectors.

Step 2. Apply Eq. (10) to the column mask to interpolate the \mathbf{y} vectors.

Step 3. To compute the missing vectors \mathbf{z} using the already interpolated vectors, apply Eq. (10) to the four directional (0 , $\pi/4$, $\pi/2$ and $3\pi/4$) masks centered on \mathbf{z} , and the mean value is assigned to \mathbf{z} .

- **VRF3_L** (*Mixed interpolation algorithm*): The two interpolator functions given by Eq. (8) and Eq. (10) can be used together in an adaptive mixed interpolation scheme as follows:

Step 1. Using Eq. (10), compute temporarily the \mathbf{x} and \mathbf{y} vectors using row and column mask, respectively.

Step 2. To compute the unknown \mathbf{z} vectors [see Fig. 2(a)], apply Eq. (8) to the two masks shown in Figs. 4(a) and 4(b), and assign the mean value to \mathbf{z} .

Step 3. Recompute the \mathbf{x} and \mathbf{y} vectors using the original vectors and the \mathbf{z} vectors computed in step 2. We apply only the mask in Fig. 4(b) and use Eq. (8) to compute the new values.

- In the case of Quincunx decimation scheme the VRF is used as follows: Considering \mathbf{a} , \mathbf{b} , \mathbf{c} and \mathbf{d} shown in Fig. 4(b) as 3-D vectors (representing the image pixels in the RGB color space) obtained from the color image by quincunx decimation method [see Fig. 2(b)]. We compute the central pixel vector using Eq. (8), with the weights given by Eq. (9) or Eq. (13).

For Modified VRFs using the directional processing (VRF_d), the corresponding algorithms are the same as for VRF1_L, VRF2_L, and VRF3_L but using the weights computed using the angles between the color vectors; hence, the notation VRF1_d, VRF2_d, and VRF3_d.

For quantitative comparison of the performance of the different interpolators, the mean absolute error (MAE), mean square error (MSE) and peak signal-to-noise ratio (PSNR) criteria are used. These criteria are defined as follows:

$$MAE = \frac{1}{MN} \sum_{i=1}^M \sum_{j=1}^N \|\mathbf{y}_{i,j} - \mathbf{d}_{i,j}\|_1, \quad (18)$$

$$MSE = \frac{1}{MN} \sum_{i=1}^M \sum_{j=1}^N \|\mathbf{y}_{i,j} - \mathbf{d}_{i,j}\|_2^2, \quad (19)$$

$$PSNR = 10 \log_{10} \frac{(255)^2}{MSE} \text{ dB}, \quad (20)$$

where M and N are the image dimensions, $\mathbf{y}_{i,j}$ is the vector value of the pixel (i, j) of the interpolated image, $\mathbf{d}_{i,j}$ is the

Table 1 Performance of the different interpolators in the case of (1/16) rectangular decimated images.

Interpolator Number	"Lena" Image				"Peppers" Image			
	MAE	MSE	PSNR	NCD×10 ⁻²	MAE	MSE	PSNR	NCD×10 ⁻²
CC	21.72	423.6	50.34	6.50	23.25	458.7	49.54	8.40
BL	19.00	351.8	51.81	6.41	22.39	418.1	50.37	8.37
VFMH	18.58	346.9	52.34	6.47	21.30	416.0	50.52	8.17
Marginal RF	18.17	340.1	52.53	6.11	21.00	375.8	51.54	7.99
VRF1 _d	18.11	331.0	52.80	6.10	20.99	374.0	51.58	7.96
VRF1 _L	18.09	329.3	52.86	6.09	20.98	372.7	51.62	7.95
VRF2 _d	18.00	326.2	52.95	6.08	20.94	371.2	51.66	7.92
VRF2 _L	17.95	325.4	52.98	6.08	20.93	369.5	51.70	7.92
VRF3 _d	17.70	314.4	53.32	6.05	20.70	364.6	51.84	7.75
VRF3 _L	17.67	313.5	53.35	6.04	20.68	362.0	51.91	7.75

vector value of the pixel (i,j) of the original image, and $\|\cdot\|_1, \|\cdot\|_2$ are the l₁- and l₂-vector norms, respectively.

To create an objective measure of the perceptual error between two color images, one must resort to objective criteria that are computed over color spaces that are related to the human perception. Precise quantification of the perceptual error between two color vectors remains one of the most important and open research problems. The RGB color space is the most commonly used color space to store, process, display and analyze color images. However, the human perception of color cannot be described directly using the RGB model.²⁰ Therefore, measures such as the MSE defined on the RGB color space are not appropriate to quantify the perceptual error between images. Thus, it is important to use color spaces that are closely related to the human perceptual characteristics and suitable for defining appropriate measures of perceptual error between color vectors. A number of such color spaces are used in areas such as multimedia, telecommunications (e.g., high definition television), motion picture production, the printing industry, and graphic arts. Among these, perceptually uniform color spaces are the most appropriate to define simple yet precise measures of perceptual errors. The *Commission Internationale de l'Eclairage* (CIE) standardized two color spaces, L*u*v* and L*a*b*, which are perceptually uniform.¹⁵ The conversion from the RGB color space to the

L*a*b* color space is explained in detail in Ref. 15. In the L*a*b* space, L* is the luminance component and a* and b* are the chrominance components.

In L*a*b* color space, we computed the normalized color difference²¹ (NCD), which is estimated according to the following expression:

$$NCD = \frac{\sum_{i=1}^M \sum_{j=1}^N \|\Delta E_{Lab}\|}{\sum_{i=1}^M \sum_{j=1}^N \|E_{Lab}^*\|}, \tag{21}$$

where ΔE_{Lab} is the perceptual color error between two color vectors and is defined as the Euclidean distance between them, given by

$$\Delta E_{Lab} = [(\Delta L^*)^2 + (\Delta a^*)^2 + (\Delta b^*)^2]^{1/2}, \tag{22}$$

and ΔL^* , Δa^* , and Δb^* are the differences in the L*, a*, and b* components, respectively. The magnitude of the original image pixel vector in the L*a*b* space is E*_{Lab} and is given by

$$E_{Lab}^* = [(L^*)^2 + (a^*)^2 + (b^*)^2]^{1/2}.$$

Tables 1 and 2 display the performance of various inter-

Table 2 Performance of the different interpolators in the case of (1/2) quincunx decimated images.

Interpolator Number	"Lena" Image				"Peppers" Image			
	MAE	MSE	PSNR	NCD×10 ⁻²	MAE	MSE	PSNR	NCD×10 ⁻²
BL	6.01	53.57	71.02	2.47	10.30	200.0	57.84	4.08
VFMH	5.89	51.18	71.47	2.44	9.86	147.0	60.92	4.05
Marginal RF	5.81	49.20	71.87	2.34	9.54	132.3	61.98	3.98
VRF3 _d	5.76	48.53	72.00	2.30	9.52	132.0	62.00	3.91
VRF3 _L	5.74	48.13	72.09	2.30	9.51	131.3	62.05	3.85

polators for the 1/16 rectangular subsampling and 1/2 quincunx subsampling, respectively. The results indicate that most of the nonlinear interpolation methods outperform the linear ones (bold-faced entries in the table indicate the best filter performance according to the corresponding objective criterion).

Based on Tables 1 and 2, we draw the following conclusions: All vector rational interpolators perform quite well, especially VRF3_L . For the two natural images used, VRF3_L and VRF3_d provide the best performance due to the maximum information collected from the known vector samples in the approximation of the missing vectors. The VRFs and the marginal RFs outperform the linear and nonlinear interpolators under consideration. Vector processing, i.e., VRF, produced better results compared to marginal (componentwise) filtering, i.e., marginal RF. The marginal RF fails to take into account the dependence between the components (i.e., the interchannel correlation), as mentioned earlier. The cubic convolution and the bilinear interpolators are inferior to all nonlinear interpolators used in the experiments. This can be easily explained as follows. Since both images used are natural and mainly composed of narrow lines, steep edges, sharp corners, etc., the bilinear filter will result in large distortions due to its smoothing properties. Obviously, any lowpass filtering is not suitable for preserving these high frequency components. The cubic convolution was applied componentwise and thus failed to use the interchannel correlation.

Although these measures are not the best in estimating the goodness of an interpolation scheme, they can still provide an idea of the relative performance of the filters. The interpolated images are presented in Figs. 7(a) to 7(f) for visual comparison since in many cases they are the best qualitative measure of performance for image processing algorithms. Figures 7(a) to 7(f) show the outputs of the bilinear interpolator, the vector FIR median hybrid interpolator, the marginal rational interpolator, and the proposed vector rational interpolators VRF1_L , VRF2_L and VRF3_L , respectively, for the rectangular decimation case of the color ‘Lena’ image. These images confirm the numerical results shown in Tables 1 and 2. The blocking artifacts are visible in the case of the bilinear interpolator. VFMH interpolation produces better reconstructed image; however, sharp edges still appear jagged. On the other hand, it is clear that the nonlinear interpolators based on VRFs and their modification are rather visually more pleasant. Furthermore, the marginal RF provides a slightly better performance than the VFMH interpolator but is still inferior to all the vector rational interpolators. The VRF3_L provides the best performance with a nearly perfect reconstructed image.

To further assess the detail preservation capability of each interpolator used, part of a horizontal row of the blue component data of the original ‘Lena’ image shown in Fig. 8(a) is used to illustrate the performance. This part corresponds to Lena’s shoulder, where the luminance smoothly increases from left to right until the steep transition to dark gray when the hair is encountered. An ideal interpolator should reconstruct the change at the shoulder-hair border without any artifact. Figures 8(b) to 8(f) represent the outputs of the bilinear, the VFMH and the proposed vector rational interpolators VRF1_L , VRF2_L and VRF3_L . From these plots, we can draw the same conclu-

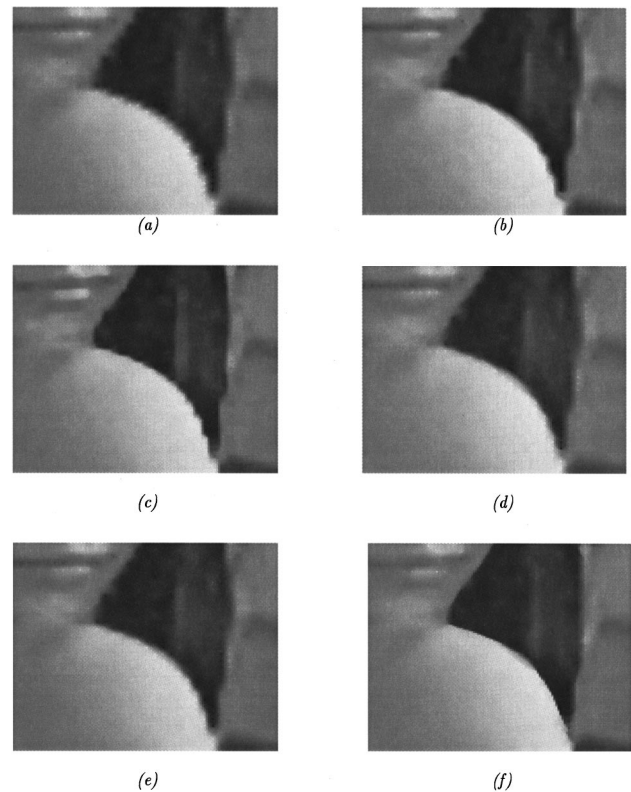


Fig. 7 Interpolated results from the (1/16) rectangular decimated ‘Lena’ image using (a) the bilinear interpolator, (b) the vector FIR median hybrid filter, (c) the marginal rational filter based interpolator, (d) VRF1_L ; (e) VRF2_L ; (f) VRF3_L .

sions as for the interpolated image in Fig. 7. We see that the VRF-based interpolators and mainly the VRF3_L provide the best edge reconstruction [Fig. 8(f)]. This confirms the result given by Fig. 7(f), where the processed image exhibits sharp nonjagged edges.

6 Conclusions

RFs are extended in this paper to the vector case and applied to color image interpolation. Two decimation schemes were used to down-sample the images, rectangular and quincunx decimation. Border-preserving and separable row-column interpolation algorithms based on VRFs were proposed and tested. A modified version of VRFs is proposed in which angle information between vectors in the filter window is used as an edge sensor. The main merits of these interpolators are their edge-preserving capabilities and the absence of artifacts normally associated with classical linear and even some nonlinear interpolation schemes.

Simulation results of the interpolated images indicate that vector rational interpolators outperform the classical linear techniques and even some nonlinear ones according to both objective and subjective criteria. In particular, VRF-based interpolators were shown to better preserve the chromaticity in the reconstructed image as measured by the NCD. Vector processing also proved to produce better re-

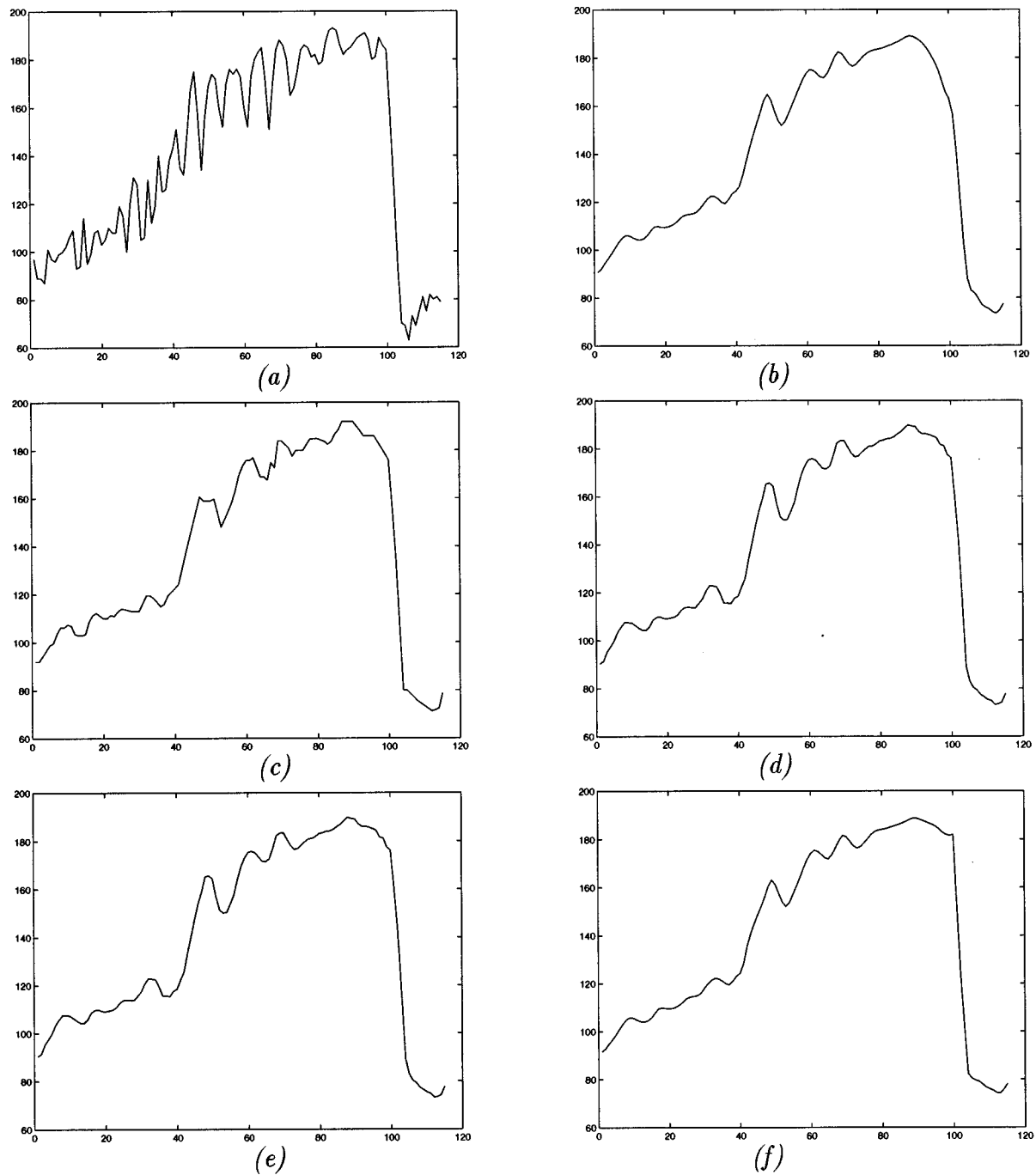


Fig. 8 Gray-level plots along an image row of the blue component data in the “Lena” image: (a) original image and reconstructed images from the 1/16 rectangular decimation technique using (b) the bilinear interpolator; (c) the VFMH filter; and the VRF-based interpolator (VRF_L), (d) VRF_{1L}, (e) VRF_{2L}, and (f) VRF_{3L}.

sults than marginal (componentwise) processing, as expected.

Acknowledgments

We would like to thank the reviewers for their fruitful comments. This work has been supported by the European ESPRIT Project LTR 20229-Noblesse.

References

1. R. A. F. Belfor, M. P. A. Hesp, R. L. Lagendijk, and J. Biemond, “Spatially adaptive subsampling of image sequences,” *IEEE Trans. Image Process.* **3**(5), 492–500 (1994).
2. H. H. Hou and H. C. Andrews, “Cubic splines for image interpolation and digital filtering,” *IEEE Trans. Acoust., Speech, Signal Process.* **26**(6), 508–512 (1978).
3. R. G. Keys, “Cubic convolution interpolation for digital image processing,” *IEEE Trans. Acoust., Speech, Signal Process.* **29**(6), 1153–1160 (1981).
4. K. P. Hong, J. K. Paik, H. J. Kim, and C. H. Lee, “An edge-

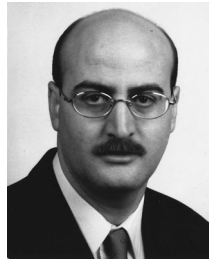
- preserving image interpolation system for a digital camcorder," *IEEE Trans. Consum. Electron.* **42**(3), 279–283 (1996).
5. F. Alaya Cheikh, L. Khriji, M. Gabbouj, and G. Ramponi, "Color image interpolation using vector rational filters," *Nonlinear Image Processing IX, Proc. SPIE* **3304**, 242–249 (1998).
 6. L. Khriji, F. Alaya Cheikh and M. Gabbouj, "Multistage vector rational interpolation for color images," in *Proc. 2nd IMACS-IEEE Int. Multiconf. on Computational Engineering in System Application: CESA'98*, p. 620 (abstract), full paper in *Proc. on CD-ROM*, Hammamet, Tunisia (1998).
 7. J. Astola, P. Haavisto, and Y. Neuvo, "Vector median filter," *Proc. IEEE* **78**, 678–689 (1990).
 8. P. E. Trahanias, D. Karakos, and A. N. Venetsanopoulos, "Directional processing of color images: theory and experimental results," *IEEE Trans. Image Process.* **5**(6), 868–880 (1996).
 9. T. Koh and E. Powers, "Second order Volterra filtering and its applications to nonlinear system identification," *IEEE Trans. Acoust., Speech, Signal Process.* **33**(6), 1445–1455 (1985).
 10. V. J. Mathews, "Adaptive polynomial filters," *IEEE Signal Process. Mag.* **8**(3), 10–26 (July 1991).
 11. G. Sicuranza, "Quadratic filters for signal processing," *Proc. IEEE* **80**(8), 1262–1285 (1992).
 12. H. Leung and S. Haykin, "Detection and estimation using an adaptive rational function filter," *IEEE Trans. Signal Process.* **42**(12), 3365–3376 (1994).
 13. J. L. Walsh, "The existence of rational functions of best approximation," *Trans. Am. Math. Soc.* **33**, 668–689 (1931).
 14. G. Ramponi, "The rational filter for image smoothing," *IEEE Signal Process. Lett.* **3**(3), 63–65 (1996).
 15. A. K. Jain, *Fundamentals of Digital Image Processing*, Prentice-Hall, Englewood Cliffs, NJ (1989).
 16. T. J. Rivlin, *An Introduction to the Approximation of Functions*, Chap. 5, p. 120, Dover Publications, New York (1981).
 17. G. Ramponi, "Image processing using rational functions," in *Proc. of the Cost 254 Workshop*, Budapest, Hungary (1997).
 18. R. Machuca and K. Phillips, "Applications of vector fields to image processing," *IEEE Trans. Pattern. Anal. Mach. Intell.* **PAMI-5**, 316–329 (1983).
 19. N. Herodoutou and A. N. Venetsanopoulos, "Colour image interpolation for high resolution acquisition and display devices," *IEEE Trans. Consum. Electron.* **41**(4), 1118–1126 (1995).
 20. W. K. Pratt, *Digital Image Processing*, 2nd ed., Wiley, New York (1991).
 21. K. N. Plataniotis, D. Androutsos, and A. N. Venetsanopoulos, "Adaptive multichannel filters for colour image processing," *Signal Process. Image Commun.* **11**, 171–177 (1998).



Lazhar Khriji received his BS degree in electronics in 1990 from the Faculty of Sciences of Tunis, Tunisia, and his MS in automation and control in 1992 from the Ecole Normale Supérieure de l'Enseignement Technique, Tunisia. He is currently a teaching assistant in the Electrical Engineering Department of the Ecole Nationale d'Ingenieurs de Monastir, Tunisia. Since March 1997 he has been a visiting researcher in the Department of Information Technology of Tampere University of Technology, Finland. His research interests include, nonlinear signal and image processing and analysis, multichannel signal processing and adaptive nonlinear filtering.



Faouzi Alaya Cheikh received his BS degree in electronics from the Ecole Nationale d'Ingénieurs de Tunis, Tunisia, in 1992. In 1993 he was an electronics engineer with the Société Tunisienne d'Electricité et de Gaz, Sousse, Tunisia. In 1996 he received his MS in signal processing from Tampere University of Technology, Finland, and he is currently pursuing doctoral studies with the Tampere Graduate School in the information science and engineering doctoral program of the Department of Information Technology at the Tampere University of Technology, where he is also a researcher at the Digital Media Institute. His research interests are nonlinear signal and image processing, content-based indexing and retrieval in multimedia databases and he is a member of the Conseil de l'Ordre des Ingénieurs in Tunisia and an IEEE student member.



Moncef Gabbouj received his BS degree in electrical engineering in 1985 from Oklahoma State University, Stillwater, and his MS and PhD degrees in electrical engineering from Purdue University, West Lafayette, Indiana in 1986 and 1989, respectively. Dr. Gabbouj is currently a professor in the Signal Processing Laboratory of Tampere University of Technology, Tampere, Finland. From 1995 to 1998 he was a professor with the Department of Information Technology of Tampere University of Technology, Pori, and during 1997 and 1998 he was on sabbatical leave with the Academy of Finland. From 1994 to 1995 he was an associate professor with the Signal Processing Laboratory of Tampere University of Technology, Tampere, Finland. From 1990 to 1993 he was a senior research scientist with the Research Institute for Information Technology, Tampere, Finland. His research interests include nonlinear signal and image processing and analysis, content-based analysis and retrieval and mathematical morphology. Dr. Gabbouj is an associate editor of the *IEEE Transactions on Image Processing* and was guest editor of the European journal *Signal Processing*, Special Issue on Nonlinear Digital Signal Processing (August 1994). He is the past chair of the IEEE Circuits and Systems Society, Technical Committee on Digital Signal Processing, and the IEEE SP/CAS Finland Chapter. He was also the DSP track chair of the 1996 IEEE ISCAS and the program chair of NORSIG'96 and is the technical program chair of EUSIPCO'2000. Dr. Gabbouj directs the International University Program in Digital Signal Processing in the Signal Processing Laboratory at Tampere University of Technology, and is a member of Eta Kappa Nu, Phi Kappa Phi, IEEE, SP and CAS. He was corecipient of the Myril B. Reed Best Paper Award from the 32nd Midwest Symposium on Circuits and Systems and corecipient of the NORSIG 94 Best Paper Award from the 1994 Nordic Signal Processing Symposium.